PAGEOPH, Vol. 131, Nos. 1/2 (1989)

0033–4553/89/020111–28$1.50 + 0.20/0

The Fractal Geometry of Flow Paths in Natural Fractures in Rock and the Approach to Percolation

D. D. NOLTE[1], L. J. PYRAK-NOLTE[2] and N. G. W. COOK[2]

Abstract—The distributions of contact areas in single, natural fractures in quartz monzonite (Stripa granite) are found to have fractal dimensions which decrease from $D = 2.00$ to values near $D = 1.96$ as stress normal to the fractures is increased from 3 MPa up to 85 MPa. The effect of stress on fluid flow is studied in the same samples. Fluid transport through a fracture depends on two properties of the fracture void space geometry: the void aperture; and the tortuosity of the flow paths, determined through the distribution of contact area. Each of these quantities change under stress and contribute to changes observed in the flow rate. A general flow law is presented which separates these different effects. The effects of tortuosity on flow are largely governed by the proximity of the flow path distribution to a percolation threshold. A fractal model of correlated continuum percolation is presented which quantitatively reproduces the flow path geometries. The fractal dimension in this model is fit to the measured fractal dimensions of the flow systems to determine how far the flow systems are above the percolation threshold.

Key words: Fractals, fractures, fluid flow, percolation, rock mechanics, geohydrology.

1. Introduction

Whether for the recovery of oil, or for the isolation of nuclear or toxic wastes, it is essential to be able to predict the rates of flow and the flow patterns of fluids in bulk rock. Substantial research has been carried out on flow through porous media, for which permeability constants are well defined. However, the case for fractured rock is not nearly as well understood. In addition to the usually isotropic permeability of the bulk rock, directional permeability must also be assigned because of the flow through fracture networks (ROBINSON, 1983). Lately, there has been special interest in fracture networks caused by the need for nuclear waste isolation, especially for the case of isolation in impermeable, crystalline rock in

[1] Department of Physics, University of California, Berkeley, CA 94720, U.S.A. Now at AT&T Bell Laboratories, Crawfords Corner Rd., Holmdel, New Jersey 07733, U.S.A.

[2] Department of Material Science and Mineral Engineering, University of California, Berkeley, CA 94720, U.S.A.

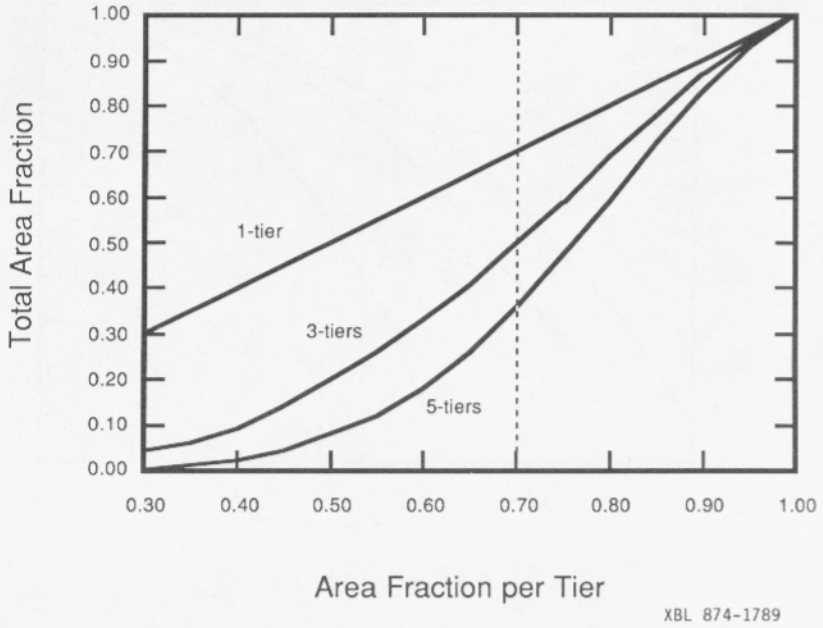

Figure 11
Approximate total area fraction as a function of $AFpT$ for a 1-tiered, 3-tiered, and 5-tiered stratified continuum percolation plot. The total area fraction is clearly a function of the number of tiers (resolution).

area fraction is the variable parameter which defines the percolation threshold and the percolation exponents. However, the total area fraction of the stratified plots is a function of the number of tiers (or the cut-off), and therefore the total area fraction is not uniquely defined. For this reason, the total area fraction of a fractal percolation model cannot be used as the critical parameter. The fractal dimension is well defined but the percolation threshold again does not occur at a uniquely defined fractal dimension: the fractal dimension can be used as an indicator of the nearness to threshold, but cannot be used quantitatively. On the other hand, the computer simulations do indicate that all the systems (for varying fractal dimension and scale factor b) have a threshold at $AFpT \approx 0.7$, which is the percolation threshold of the standard model. A well defined percolation threshold can therefore be identified for the stratified percolation simulations which use AFpT as an input parameter.

Defining the percolation threshold is of great importance for helping understand the flow properties of a random system. Near the threshold, the flow equation should be

$$Q - Q_\infty = C \cdot (d_{\max} - d)^m \cdot (AFpT - 0.7)^t \tag{8}$$

where t is the flow percolation exponent. Extensive Monte Carlo renormalization

Questions about the effect of changing contact area and increasing tortuosity on fluid flow fall under the realm of percolation theory. This theory takes as its input the results of the topography of the flow paths, including both aperture and contact area distributions. The main goal of this paper is to directly image the changing contact area under applied stress and extract the effect of changing contact area alone on the fluid flow rate by relying on the results of two-dimensional percolation theory. In Section 2, we present direct measurements of flow path patterns in natural fractures. We also provide data of the fluid flow rate through the fracture as a function of the fracture closure in order to correlate flow rate with the flow path patterns. The flow path geometry is defined through the distribution of contact area, which is describable by fractal dimensions, discussed in Section 3. The flow area fractions and fractal dimensions are used to construct a two-dimensional correlated continuum-percolation model in Section 4.

2. Experimental Data

We studied the deformation and flow properties of fractures in three separate core sections of quartz monzonite (Stripa granite (OLKIEWICZ *et al.*, 1979)) which were 52 mm in diameter by 77 mm in height. These cores were obtained from extensometer holes from a waste isolation experiment in a drift in Stripa, Sweden, 340 meters below the surface. The fractures are orthogonal to the core axis. The core samples are labled E30, E32, and E35, corresponding to the extensometer holes from which the cores were derived. The closure of the fractures under applied stress was measured by linear variable differential transformers (LVDT's). The mechanical deformation data for the samples are given in Figure 1. The stiffnesses of the fractures are defined from the inverse tangents of the deformation curves. At 20 MPa normal stress, the stiffnesses are: E35, 3×10^{12} Pa/m; E30, 7×10^{12} Pa/m; and E32, 15×10^{12} Pa/m. The stiff fracture in E32 deforms to a value of $d = 5.5$ microns, while the compliant fracture in E30 deforms considerably more to $d = 9.5$ microns at normal stresses of 85 MPa. The fluid flow data through the fractures as a function of the fracture closure are presented in Figure 2. There is a clear correlation between fracture stiffness and fluid flow in that the stiffer fractures support less flow. Under even the highest stresses, there remains an irreducible flow, denoted as Q_∞. By analogy with the cubic law described by eq. (1), we fit the flow data to the equation

$$Q = Q_\infty + C(b_{\text{mech}})^n \tag{2}$$

where $b_{\text{mech}} = (d_{\max} - d)$ is called the mechanical aperture. The quantity d is the measured closure for a given applied load, and n is the flow exponent. The maximum mechanical closure of the fracture is $d_{\max}$, which can be understood as the average aperture which results when there are only three points of contact between the two fracture surfaces at zero normal load. The values for $d_{\max}$ are fit from the

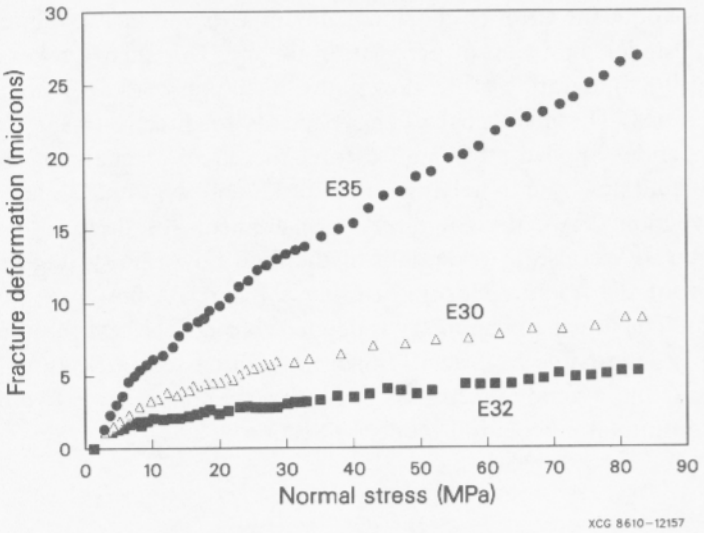

Figure 1
Mechanical closures of three fractures as functions of applied stress. The stiffnesses of the fractures are equal to the tangent slope of the deformation curves.

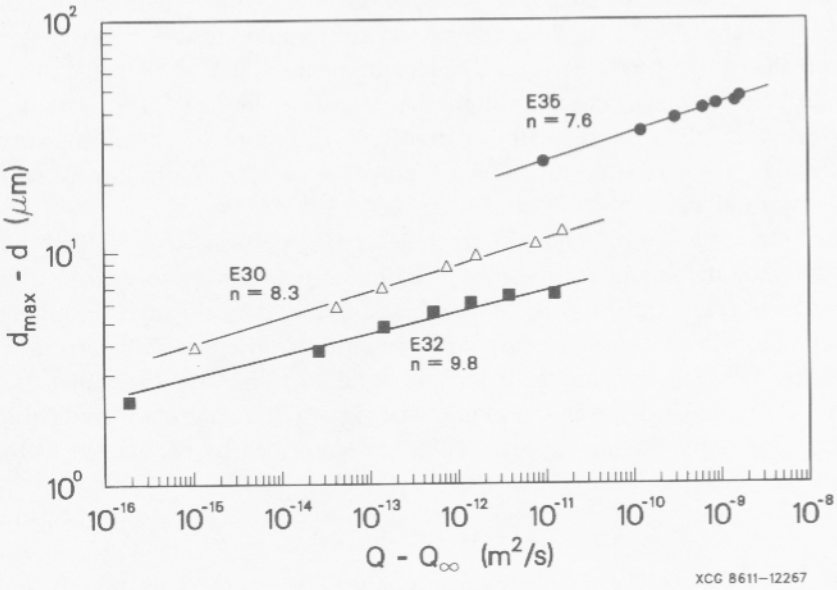

Figure 2
Hydraulic flow per unit head as a function of mechanical fracture closure for the three fractures. The compliant fractures support greater flow than the stiff fracture, as expected. The irreducible flow, Q_∞, is that flow which remains when the fracture is hydraulically closed. The solid lines fit eq. (2) to the data for the given exponents, n. All exponents are much greater than cubic.

data: for E35 $d_{max} = 46$ microns; for E30 $d_{max} = 12.5$ microns; and for E32 $d_{max} = 6.6$ microns. The quantity Q_∞ is the irreducible flow, defined as that flow which remains when the maximum closure d_{max} has been reached. We consider this flow to result from permanent conduits carved in the fracture surface which are virtually unaffected by applied stress. This flow therefore occurs in parallel with the flow occurring over the fracture surfaces. Even parallel plates could have irreducible flow if there were small interconnected grooves in the plate surfaces. Experimental data for flow between ground quartz surfaces under high stress does, in fact, show this (ENGELDER and SCHOLZ, 1981).

Although eq. (2) is reminiscent of the cubic law, there is no reason, *a priori*, to believe that the exponent n should have a value near 3. Part of the difficulty in applying the cubic law to fracture lies in the problem of how to define an appropriate average aperture. The mechanical aperture defined above for the mechanical closure of a fracture under applied stress is likely to differ from an average hydraulic aperture defined by a weighted average over directly measured aperture profiles. In fact, mechanical aperture may not even be linearly proportional to hydraulic aperture (PYRAK-NOLTE *et al.*, 1987), and this could influence the exponent n measured for mechanical closure. Despite these difficulties, we emphasize and use mechanical aperture over aperture distributions obtained from profile or thin-section measurements because of the ease with which this data is obtained (requiring only a single deformation experiment compared to multiple profiles or thin-sections). Furthermore, the mechanical closure of a fracture is measured unambiguously, while aperture profiles require complicated statistical analyses in order to predict their effect on fluid flow. The use of the empirical eq. (1) should therefore simplify the process of fracture characterization, and speed up the prediction of flow properties in the field based on core samples measured in the laboratory. What remains is to explain the exponent n. The values of n in eq. (2), shown for different fractures in Figure 2, are found to lie near $n \sim 8$, much larger than cubic or even quartic (which holds for flow in a tube). Such strong deviations from the cubic law imply that the flow properties of these natural fractures must be heavily influenced by the effects of the flow path topology.

Despite the fact that changes in the contact area as a function of stress can have a pronounced effect on the flow properties of the fractures, fracture contact area has been an elusive and very difficult parameter to measure and image. Various indirect means have been tried previously to observe the contact area (DUNCAN and HANCOCK, 1966; IWAI, 1976; BANDIS *et al.*, 1983), with varying degrees of success. We have used a new technique (PYRAK-NOLTE *et al.*, 1987) developed to make a direct measurement of the contact area of fractures. This technique involves injecting molten Wood's metal into fractures which are initially evacuated. During the injection, stress is maintained on the fracture through a servo-controlled, stiff-testing machine. The pore pressure of the molten metal was maintained at 2 MPa through the injection and cooling of the cast in the fracture. The effective

stress on the fracture is calculated by subtracting this confining pressure from the applied load. After the metal cools, the fracture is taken apart, revealing a direct metal cast of the fracture void space. The metal adheres to either one or the other surface of the fracture, tearing along lines of contact between the rock surfaces. It was observed that the metal on one surface does not overlap with the metal on the other at the same location. The damage inflicted on the metal cast by tearing was observed under an electron scanning microscope to be limited to only several microns at most. In fact, SEM micrographs of the separate surfaces, probing sections 0.25 mm on a side, could be superposed with high accuracy, fitting together with minimal overlaps or gaps between the metal patterns on the two surfaces.

Images of the metal casts of the void spaces for E30 and E32 under 3 MPa, 33 MPa, and 85 MPa are shown in Figure 3. A computer enhanced composite of

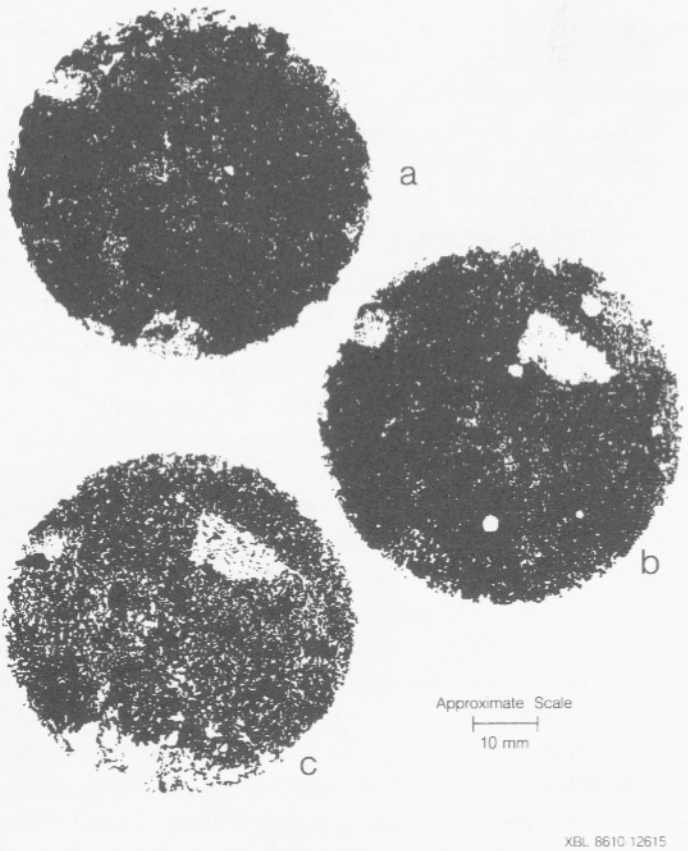

Figure 3.1
Contact area composite images for sample E30 for (a) 3 MPa, (b) 33 MPa, and (c) 85 MPa. The black portion is the flow path geometry; the white areas are the contact area. The resolution of the patterns is about 3% of the diameter.

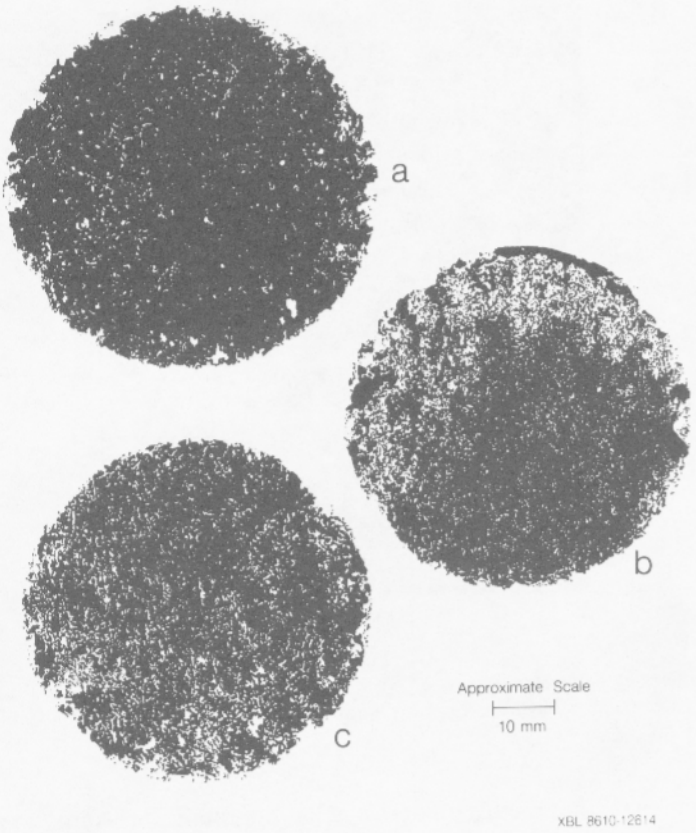

Figure 3.2
Contact area composite images for sample E32 for (a) 3 MPa, (b) 33 MPa, and (c) 85 MPa.

scanning electron micrographs of the two fracture surfaces of sample E30 under 85 MPa at 25 times magnification is shown in Figure 4. This figure represents an area 2 mm by 4 mm of the fracture. The error in this figure, caused by possible misalignment of the SEM micrographs or damage to the metal cast, is less than 1%. The hydraulic void space is black, while the contact area is white. As the stress is increased, the amount of contact area increases, producing barriers to flow which force the flow paths to become more tortuous. Large, single areas of contact are observable for the compliant fracture in E30, but are absent for the stiff fracture in E32. There is an important connection between the observed contact area and the surface tension of the injected metal. Specifically, a fluid with a given surface tension and at a given confining pressure can only enter into apertures larger than a certain size. This, in fact, is the principle on which mercury porisometry is based: by injecting mercury into porous or fractured media under different confining pressure, one can measure pore and void space volume. Calculations for molten Wood's

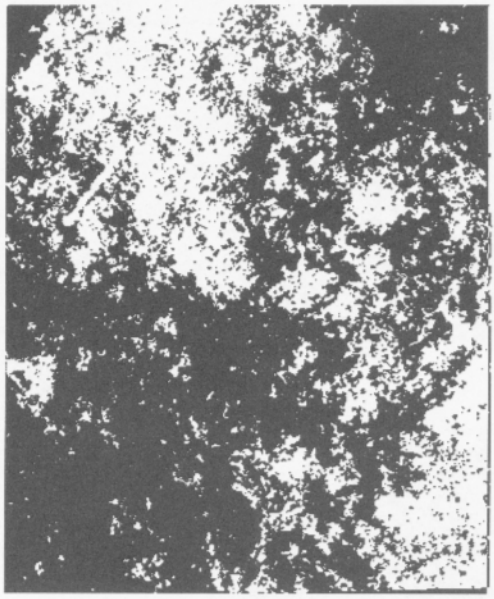

XBL 8611-4760

Figure 4
A computer enhanced composite image of SEM micrographs of E30 at 85 MPa under 25 times magnification. The area of the figure is 2 mm by 4 mm. The fractal dimension of this section is $D = 1.93$.

metal predict that the metal, under 2 MPa confining pressure, can penetrate apertures on the size of tenths of a micron. In the SEM micrographs, filaments of the metal as small as 0.2 microns wide were observed. We consider this to be the smallest aperture which the metal can penetrate. The ability of the metal to penetrate small apertures is further borne out by the observation of areas in Figures 3 and 4 which are covered by metal, but which are surrounded entirely by contact area (at least to the resolution of the figures). This is a good indication that we are sampling nearly the entire void space of the fracture. The contact area fractions were measured using a Zeiss image analyzer. The resulting area fractions of void space are presented in Figure 5 as a function of stress. The error bars on the figure represent the uncertainties inherent in the image analysis, related to the scaling properties of the flow paths. In fact, fractal structures (we show later in this paper that the flow paths are fractal) are not required to have well-defined areas, rather the areas may depend on the resolution (or lower cut-off) of the pattern. This will be discussed in more detail later. For our resolution (3% of the diameter for the large composites), the void area fraction of the stiff fracture approaches a constant value at fairly low stress, while the void area fraction of the more compliant fracture continues to decrease up to 85 MPa. The void area fraction of flow of the stiff fracture is substantially smaller than the area fraction of the compliant fracture

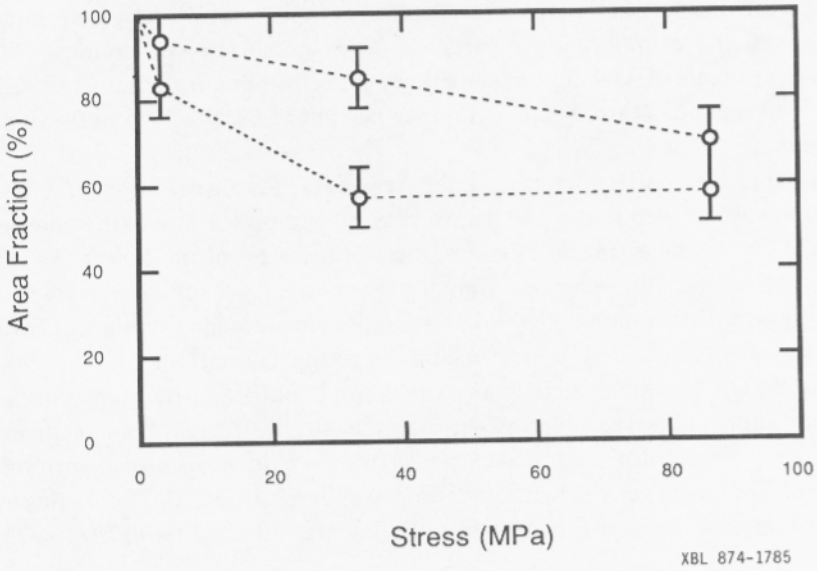

Figure 5

The flow area fraction as a function of stress for the two samples at the resolution given in Figure 3. The area fraction is usually one of the few directly measurable parameters which can enter into percolation theory analysis. For fractal patterns, however, the area fraction may not be uniquely defined.

despite the absence of the large, bulky areas of contact which are present in the pattern of the compliant fracture. This indicates that the areas of contact of the stiff fracture are considerably more stretched out and filamentary than the areas of contact of the compliant fracture. These differences between the two fractures are likely to be a consequence of the low aspect angles of the void spaces in the stiff fracture compared to the high aspect angles in the compliant fracture. It is furthermore important to point out that the stiff fracture has greater contact area than the compliant fracture, and has correspondingly less flow.

Perhaps the most interesting features of the flow path geometries, and the most relevant to the flow properties of the fracture, are the distributions and shapes of the contact areas and flow paths. While the patterns certainly appear random, they have an unmistakable scaling structure which implies they might be fractal. This possibility is explored in the next section, and the patterns are, in fact, found to have fractal dimensions which vary with the applied stress.

3. Fractal Geometry of the Contact Area

There has been strong interest in the ability of fractal geometry to describe many of the characteristics of seemingly structureless patterns (MANDELBROT, 1983).

Much of this interest has come after the realization that an impressive number of random systems exhibit scale invariance, also known as self-similarity; that is, certain parameters describing the system (or pattern) remain the same regardless of the scale of magnification. Scale invariance lies at the heart of the notion of fractal dimension.

For a random pattern to have scale invariance, the distribution of the sizes of the features which define the pattern must vary as a power law with some scale, b: $P(b) \propto b^{-(D+1)}$. The exponent D is the fractal dimension of the object. As such, the concept of fractal dimension is simply the consequence of power-law statistics governing size distributions. Power-law statistics ensure scale invariance. Invariance under transformation is a powerful and recurring concept in physics describing widely different phenomena. In many of these phenomena, invariance under scale transformation offers valuable insight into the physical origins of the phenomena and often provides for the use of powerful analytic tools for describing their structure. For instance, the scale invariance of fractal objects allows the analytic results of renormalization group theory (DOMB and GREEN, 1976; MA, 1973) to be used.

In application, real systems rarely possess the same scaling properties for all scales. Namely, there are scales above or below which the scaling properties change. These scales are called cut-offs. Often the cut-offs can carry as much information about the physical processes creating the pattern as the scaling properties of the patterns. Typically, when a fractal dimension is assigned to a pattern, this dimension is only valid for scales above a lower cut-off and below an upper cut-off. In fact, measurement of certain fundamental properties, such as contact area, depends directly on the cut-offs. Also, the measurement of the fractal dimension can be influenced by cut-offs when the measurement scale approaches the cut-off scale. For these reasons, particular attention must be paid to the limits of the regimes of scaling when attempting to define the physical properties of a pattern.

With the power of fractal description comes considerable complexity. Fractal objects take on a tremendous variety of forms, and sometimes several fractal dimensions can be defined for the same object. For example, a random percolation network (in two dimensions) at its critical percolation threshold has a fractal dimension of $D = 1.89$ (AHARONY, 1984; STANLEY, 1977). At the same time, the fractal dimension of the backbone of the percolating cluster (the backbone is defined as that part of the cluster which carries flow, *i.e.*, dead-ends are excluded) is $D = 1.59$ (AHARONY, 1984; SCHLIFER *et al.*, 1979). Similarly, in the case of the fracture flow paths, many fractal models can be used to describe the void-space topology. Because the main goal of this paper is to understand the effects of the two-dimensional contact area on flow through fractures, we only consider two-dimensional fractal models, neglecting for the moment possible fractal models for aperture distributions. Although several different models could be considered, we find one fractal model particularly relevant and easy to relate to the observed flow

path patterns: the fracture contact areas can be viewed as random holes, or tremas (MANDELBROT, 1983), which puncture a conductive sheet. Therefore the flow paths can be modeled as lying on a random Sierpinski carpet.

A random Sierpinski carpet, shown in Figure 6, is constructed iteratively by removing successively smaller squares (or tremas) from the original black square. In the carpet shown, 8 out of 9 sub-squares, of scale $b = 1/3$, remain at each level. This gives the carpet the approximate fractal dimension $D = \ln 8/\ln 3 = 1.89$. The fractal dimension of a Sierpinski carpet can be measured, in principle, by counting the number of tremas (single areas of contact) with area, a, larger than some set value, A. In practice, the counting is carried out by superposing grids with successively smaller spacings and counting the number of grid squares at each level which are occluded more than 50% by a single trema. The fractal dimensions are derived from the slope of $\ln(b^2 - N)$ vs. $\ln b$, where b is the scale size of the grid and N is the number of squares occluded for that scale b. The quantity $(b^2 - N)$ is the number of grid squares which remain uncut by tremas at this scale size. The fractal dimensions for the large composites in Figure 3 of samples E30 and E32 are shown in Table 1. The largest grid size was 32 mm, corresponding to the scale $b = 1$. The resolution of this analysis for these large composites is 1 mm, corresponding to scale $b = 32$. Upper and lower cut-offs are defined as lengths above and below which the pattern ceases to scale, and therefore appears homogeneous. SEM micrographs of the flow patterns under 200 times magnification show a clear

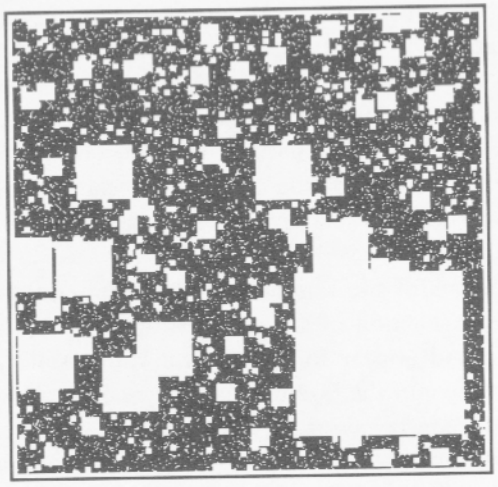

XBL 8611-4762

Figure 6
A random Sierpinski Carpet with the approximate fractal dimension $D = \ln 8/\ln 3 = 1.89$. In the limit of true scaling, the black portion vanishes.

Table 1

*Measurement of fractal dimension of flow area. Area fraction ($b^2 - N$) as a function of scale size**

Scale $1/b$	E30			E32		
	3 MPa	33 MPa	85 MPa	3 MPa	33 MPa	85 MPa
1 sample size	1	1	1	1	1	1
1/2	4	4	4	4	4	4
1/4 cut-off	16	14	14	16	16	16
1/8	64	59	59	64	59	60
1/16	253	233	225	255	234	229
1/32 resolution	1016	922	894	1014	916	925
$D =$	1.996	1.975	1.964	1.997	1.955	1.955 ± 0.01

* Scale $b = 1$ corresponds to 32 mm.

change in the void-space morphology. This is not surprising because at these length scales the surface tension of the injected metal prevents the metal from penetrating void spaces smaller than 0.2 μm. Also, the grain size of the crystalline quartz monzonite is comparable in size to, or larger than, these length scales. Therefore the lower cut-off of the flow pattern may be expected to lie somewhat above 5 microns. Similarly, an upper cut-off occurs at sizes comparable to the size of the sample. This change in scaling behavior can be seen in Table 1 to occur at a grid size of 4 mm. For grid sizes larger than this, the pattern appears homogeneous and has the corresponding fractal dimension $D = 2$. For grid sizes smaller than this, the pattern scales with a characteristic fractal dimension less than 2. The change in scaling between 4 mm and 8 mm is in agreement with work that has found correlation lengths on the order of millimeters between the two surfaces of a natural fracture (BROWN *et al.*, 1986). This upper cut-off may be an artifact of the experiment related to sample size. To test this, the scaling properties of metal injection in larger core samples should be investigated.

The fractal dimensions of the samples (in the regime in which they scale) are plotted in Figure 7 as a function of stress. The fractal dimensions clearly decrease with increasing stress, and appear to approach a value near $D = 1.95$. It is likely that the flowpath geometry in the fractures is only fractal to lowest order, and that deviations from true scaling behavior may be anticipated. As a check of the fractal dimensions calculated for the large composites (down to 1 mm length scale), the fractal dimension was calculated for the SEM micrograph shown in Figure 4 of Sample E30 at 85 MPa for 25 times magnification. We investigated a section of this micrograph 2 mm on a side with a smallest resolution of 60 microns. These sizes are substantially below the upper cut-off of 4 mm and therefore the fractal dimension

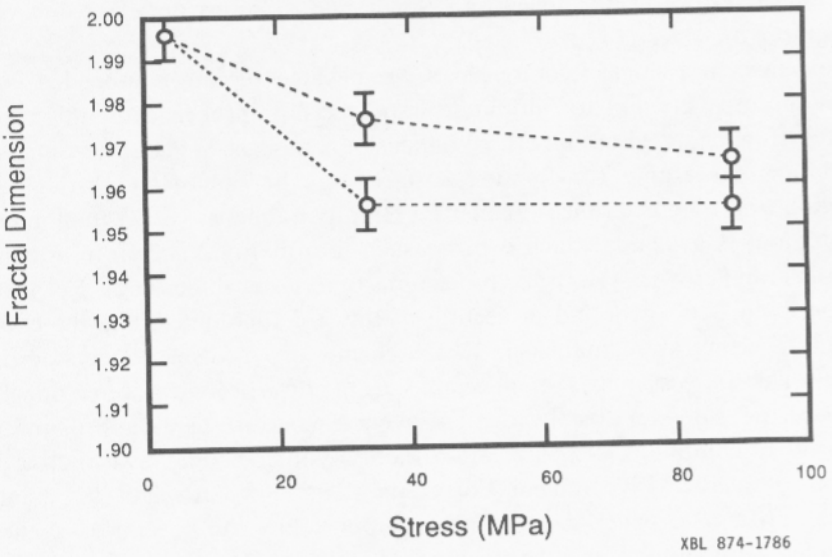

Figure 7
The fractal dimensions of the flow paths as functions of stress. The fractal dimensions of both fractures depend nonlinearly on stress and appear to asymptote to values near $D = 1.95$.

at this scale should not be influenced by the cut-off. The results of the measurement are shown in Table 2. The fractal dimension of this section was measured to be $D = 1.93$. This value is smaller than the value $D = 1.96$ measured for the same sample at lower resolution. This error may be due to simple fluctuations from site to site on the fracture, but may also be an indication that the fractal dimensions calculated for the large composites are artificially increased by their proximity to the

Table 2

*Measurement of fractal dimension of SEM micrograph. Area fraction as a function of scale size**

Scale $1/b$	$(b^2 - N)$
1	1
1/2	3
1/4	13
1/8	50
1/16	193
1/32	741
$D =$	1.93 ± 0.01

* Scale $b = 1$ corresponds to 2 mm.

upper cut-off. However, the deviation is small, and to lowest order the flow pattern does appear to scale.

Fluid flow in a single fracture has a complicated topology imbedded in three dimensions. Any attempt to fully understand the flow properties of this topology must therefore be based on fully three-dimensional models. While three-dimensional information concerning the fracture surface may be obtainable through stereo projection or profilometer measurements, currently no theory (other than numerical computation) is available which can use such information. Therefore attempts to define this topology must resort to projections onto lower dimensions. For instance, our flow path data is the 2-d projection of this 3-d topology, while the effects of changing aperture are contained in measurements of 1-d displacements across the fracture. The simplest model which establishes the flow process in three dimensions multiplies the 2-d flow area by the 1-d average aperture. This approximation is equivalent to combining 2-d percolation theory with the cubic law. Such a model must be considered as incomplete. For example, the flow-path data is presented as a binary process in which regions either support flow or not. In fact, the flow constitutes a continuum, and the flow area fraction is a function of the threshold. In our experiment, that threshold is set ultimately by the surface tension of the injected molten metal. In addition, the assumption of an average aperture can grossly oversimplify the effects of changing aperture distributions. Changes in the fracture aperture, even at relatively low stresses, can dramatically alter the critical flows paths (defined as those paths which carry the bulk of the flow), changing the flow substantially more than would be expected for the case of flow between parallel plates. Despite these difficulties, the simple model provides a starting point for deriving a general flow equation whose parameters can be established empirically. To begin, it is necessary to separate the two-dimensional flow properties from the effects of changing aperture. This is achieved in the next section.

4. The Approach to Percolation

In fitting the flow data of Figure 3 to eq. (2), all effects of the changing flow path topology were implicitly included in the fracture closure. We now consider the closure and the flow area fraction separately. To do this, we discard for the moment the flow continuum, and consider only a binary process in which flow is either present or not. The effects of 2-d flow path topology on flow properties can be largely understood from percolation theory (KIRKPATRICK, 1973; STAUFFER, 1980; ESSAM, 1980). Standard percolation theory is performed on a lattice of sites connected by bonds. The number of bonds entering a site is called the coordination of the lattice. The lattices can be two-dimensional or three-dimensional, or have even larger integer dimensions. The two basic forms of percolation models are site-percolation and bond-percolation. In site percolation, the sites are occupied

with a probability, p_s. No flow can occur through an unoccupied site. In bond percolation, the bonds are occupied with a probability p_b, and no flow can occur through an unoccupied bond. The fundamental property of a random flow system is the existence of a critical probability, p_c, which defines the percolation threshold. For occupation probabilities below the critical probability, no connected path exists through the random network and the conductivity is zero. At the percolation threshold, only a single percolating cluster exists. This percolating cluster has a fractal dimension of $D = 1.89$. For values of the occupation probability increasing above the critical density more connected paths can be found, and the conductivity increases sharply. The critical probability is a function of the lattice dimension, and also of the specific model (site vs. bond). The qualitative trend of the conductivity as a function of density is shown in Figure 8. The power of percolation theory comes from its ability to define the critical threshold parameter (PIKE and SEAGER, 1974), as well as the functional form of the conductivity near the percolation

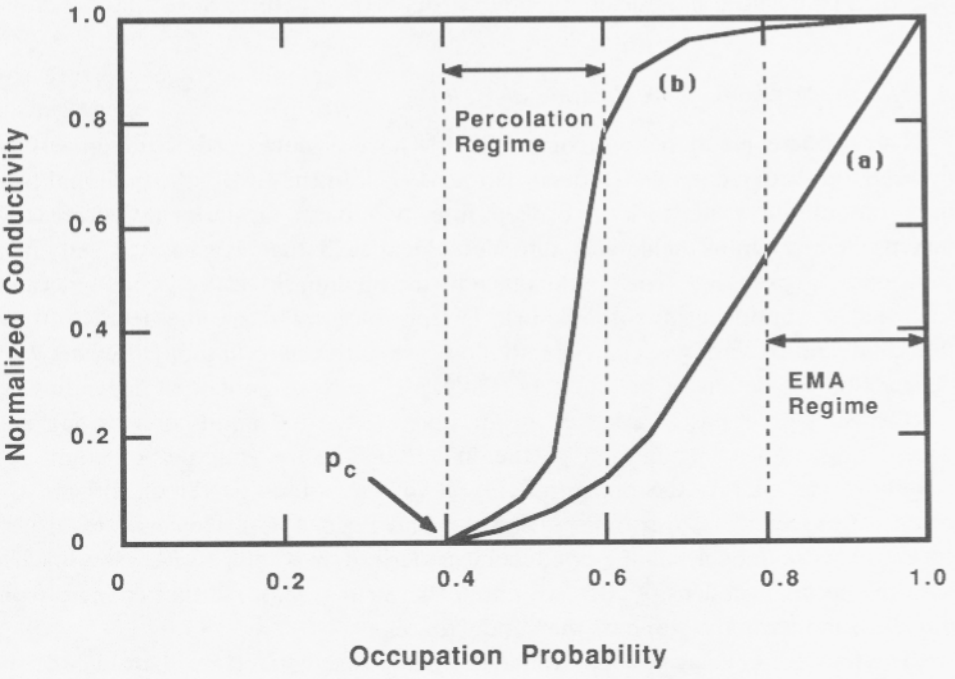

Figure 8

Conductivity as a function of the occupation probability for characteristic percolation systems. The curves represent the behavior for binary aperture distribution (a) and for continuous aperture distribution (b) (from SEAGER and PIKE, 1974). The region slightly above the percolation threshold, p_c, is the percolation regime in which the conductivity is described by a power law with an exponent, t. The region near unit occupation probability is the regime of the effective medium approximation (EMA) in which the conductivity depends linearly on the occupation probability p.

threshold. Because of scale invariance at the percolation threshold, the conductivity slightly above the critical threshold obeys a power-law-relation as a function of density: $\sigma \propto (p - p_c)^t$, where p is the flow path density, p_c is the critical density, and t is the conductivity exponent. As the system moves far above the percolation threshold, the random flow network can be characterized by applying the effective medium approximation (EMA) (KIRKPATRICK, 1973) from which a homogeneous conductivity can be defined for the system. The EMA region of Figure 8 occurs near unit density.

Under the application of stress, the fracture contact area increases, presenting barriers to flow and forcing the flow paths to take on increasingly tortuous routes. We first consider the effective medium approximation and its results for a general flow law as a function of stress. We then turn to percolation in a continuum in order to model the flow paths observed empirically. Developing a model which reproduces the qualitative and quantitative features of the experimentally observed contact areas should provide insight into the interplay between frature morphology and flow path geometry. But most importantly, such a model can be used to quantitatively estimate the critical threshold parameter for flow through the fracture.

A. Effective Medium Approximation and Flow

The effective medium approximation (EMA) was developed to describe flow through a disordered system (KIRKPATRICK, 1973). In the EMA, the potential field in a random flow network is broken into two parts: a uniformly decreasing macroscopic potential field, and a random local field that averages to zero in a sufficiently large region. The conductance of the medium is set to a constant value such that the uniform macroscopic field is reproduced. The specific details of how the conductance varies as barriers to flow are introduced into a flow network depends on the details of the network. Different results are obtained depending on whether sites or bonds in a lattice are occupied (site- and bond-percolation), and depending on the coordination of the underlying lattice (number of connected neighbors), as well as the dimensionality (two dimensions or three), and on the details of the aperture distribution (SEAGER and PIKE, 1974). However, regardless of the network model, all the conductances derived from the EMA vary linearly with the occupation density (BÖTTGER and BRYSKIN, 1985). All that changes from model to model is the slope of the conductance.

The flow eq. (2) can now be expanded for the case when $AF \sim 1$ to include the effect of changing area fraction:

$$Q - Q_\infty = C \cdot (d_{\max} - d)^m \cdot (r \cdot AF + (1 - r)) \tag{3}$$

where the second term in parentheses is the two-dimensional normalized conductance which depends linearly on the occupation probability (total flow area fraction, AF) with the slope r. The quantity $(1 - r)$ is the y-intercept, C is an

arbitrary constant, and Q_∞ is the irreducible flow. The physical content of the above equation lies mostly in the exponent, m, and in the slope, r. We have insufficient data to define the functional form of the flow area fraction in order to fit either of these parameters accurately. However, the overall effect of including the area fraction in eq. (3) is to reduce the values of the exponents m from the values of n cited before. Rough estimates of m, however, indicate that the exponents are only reduced from $n \approx 8$ in eq. (2) to $m \approx 7$ in the above equation. In fact, the effective medium theory neglects the true three-dimensional character of the flow topology. The large exponents suggest that critical flow paths are changing more dramatically, even at low stresses, than for flow between parallel plates. In addition, it is clear from considering the tortuous flow paths in Figure 4 that under the highest stresses the flow paths must be approaching the percolation threshold. Therefore to characterize the flow properties of the fractures at all stresses it is necessary to consider the results of percolation theory.

B. Continuum Percolation

In order to estimate the effects of percolation, it is essential to know the critical area fraction for percolation. The most realistic percolation model should certainly be a continuum model (PIKE and SEAGER, 1974; ELAM *et al.*, 1984; PHANI and DHAR, 1984) because there is no physical basis for assuming an underlying lattice for the fracture. Continuum percolation is a fairly recent extension of the standard lattice percolation models, and therefore its properties have not been as extensively studied. However, continuum percolation is assumed to be in the same universality class as lattice percolation (VICSEK and KERTESZ, 1981; GAWLINSKI and STANLEY, 1981; BALBERG *et al.*, 1983), so many of the standard results are expected to hold for continuum percolation as well.

One possible model for the flow paths in the fractures involves randomly distributing circles in the plane. The occupied area fraction in this model is (PIKE and SEAGER, 1974)

$$AF(N) = 1 - \exp\left[-\frac{N\pi r^2}{\text{Area}}\right] \tag{4}$$

where r is the radius of the circles, and Area is the area in which N points are placed. The quantity in the exponential is simply the mean number of centers that fall within an area of radius r. The critical area fraction for the onset of percolation has been determined to be $AF_c = 0.688$ (PIKE and SEAGER, 1974), which corresponds to the mean value of 1.14 points per circle of radius r. A percolation plot near the percolation limit with $AF = 0.7$ is shown in Figure 9.

Because continuum percolation is assumed to be in the same universality class as lattice percolation, the mean size of the percolation clusters (correlation length) is expected to be the same if the occupation probability of lattice percolation is replaced by the area fraction (ELAM *et al.*, 1984; GAWLINSKI and STANLEY, 1981).

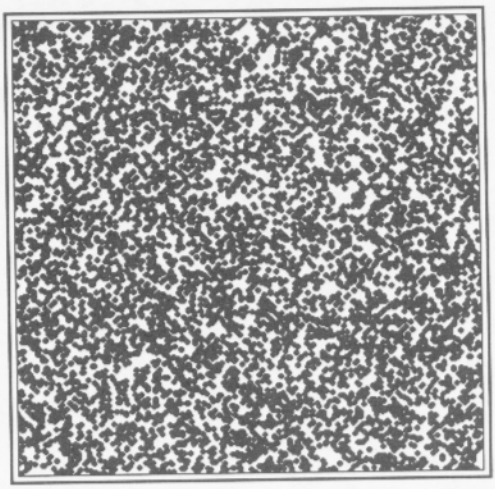

XBL 8611-4761

Figure 9
A random percolation plot near the percolation limit with area fraction $AF = 0.70$. The pattern cannot qualitatively reproduce the aggregated structures of the real flow path data in Figure 4. Specifically, the fractal dimension of the percolation plot is $D = 2.00$ regardless of the area fraction.

The conductivity exponent, t, defined by $\sigma \sim (p - p_c)^t$, is a different matter. The conductivity exponent in lattice percolation is the same for both electrical conductivity and for fluid conductivity because all the bonds have equal apertures. The accepted value is $t = 1.2$ for 2-d (BÖTTGER and BRYSKIN, 1985). However in continuum percolation the flow paths have different apertures, which affects the flow of electrical and fluid currents differently. These differences were investigated theoretically by HALPERIN *et al.* (1985) for a Swiss-cheese model in which circular holes were randomly punched in a two-dimensional conductive sheet. They found a substantial increase in the value of t for fluid flow over the value from lattice percolation. This was attributed to the cubic dependence of fluid flow on aperture which caused the narrow flow necks to dominate the fluid flow properties. The values of t were found to be model dependent, but the new estimates of t for fluid flow in a two-dimensional continuum ranged from $t \sim 1.7$ to 2.7.

This critical exponent for flow could be used to model the flow for values of high stress. However, several deficiencies exist in the random continuum percolation model for the flow paths through a natural fracture. At the highest stress, the area fractions of E30 and E32 are 0.69 and 0.59, respectively. From the random continuum percolation model the critical area fraction is 0.68 which would imply that E30 just barely percolates, while E32 is unable to support flow. Yet a cursory inspection of the flow paths shows that substantial flow is present at these values of area fraction. In addition, the random percolation plot of Figure 9 cannot qualitatively reproduce the large areas of contact in sample E30. Finally, for random

percolation, the fractal dimension of the entire pattern (percolating as well as nonpercolating clusters) is equal to 2.00 (only the single percolating cluster at threshold has a fractal dimension $D = 1.89$). However, we have already demonstrated that the complete flow path patterns have fractal dimensions at all values of stress.

C. *Stratified Continuum Percolation*

An improved continuum percolation model can be constructed by considering the auto-correlation function of the percolation plots. For random percolation, if a given site is occupied, the probability that a site which is a distance R away is also occupied is independent of R. From an inspection of the contact areas of the fractures, however, it is apparent that sites of contact have a high probability of being immediately surrounded by other sites of contact. In other words, the contact area is self- or auto-correlated. Correlation and fractal dimension are directly related. The auto-correlation function of a distribution $f(r)$ is defined by

$$F(R) = \int f(r)f(r + R)dr \tag{5}$$

where $F(R)$ is the probablity that a feature of $f(r)$ present at site r is still present at site $r + R$. If $f(r)$ represents a power-law probability distribution, then the distribution is fractal, and its auto-correlation function varies as $F(R) \sim R^{-m}$, where $m = E - D$, and E is the Euclidean dimension. For the random continuum model, the auto-correlation function is a constant, which gives a fractal dimension $D = 2.00$. Therefore, a better model for the flow paths through the fractures should be a continuum percolation model that possesses correlations. Aspects of correlations in percolation models have been considered for nearly as long as percolation theory itself (PIKE and SEAGER, 1974). But the assumed interactions have been short-ranged, extending only to the first few nearest neighbors (KLEIN, 1982; TUTHILL and KLEIN, 1983). The correlation functions of these models do vary with R, but they do not scale (except at the critical threshold), which is required for the models to be fractal.

There are several ways to introduce correlations into percolation models. One approach transforms an originally random distribution of sites into a new plot according to defined rules that act to clump the occupied points. Different transformation rules produce different correlation functions, and the rules can be adjusted to fit the empirical data. However, this procedure is not easily implemented for a continuum model, and the properties of the resulting plots have no obvious connection to the properties of the random model. We choose a different approach which produces percolation plots that scale with adjustable fractal dimensions, but which preserves some of the properties of the standard continuum percolation model. This percolation model is a hybrid between a Sierpinski carpet and the

random percolation plot, and is constructed iteratively, with the standard continuum construction applied at each iteration. The procedure begins by randomly distributing N sites within a given square region, called a tier. Each site defines the center of a new tier which is smaller, by a scale factor b, than the parent tier. Within each of the new, smaller tiers, N points are randomly distributed which define the centers of yet new tiers that are again reduced in size by a factor of b from the immediately preceding tier. The procedure continues for as many iterations as is necessary, or possible, within the resolution of the graphics. At the last iteration, the squares of size $1/b^n$ are finally plotted, where n is the number of tiers. This model is a stratified continuum percolation model.

The fractal dimension of the pattern is estimated by considering the area fraction at each stage. Because the distributions are allowed to overlap, double counting must be avoided in the calculation of the area fraction. Starting with a given area fraction per tier, $AFpT = AF(N)$ (defined in eq. (4)), the fractal dimension is approximately

$$D \approx \frac{\ln[AFpT + (1 - AFpT)(AFpT)^2]}{\ln[b]} + 2. \tag{6}$$

In the absence of overlap, the fractal dimension would be $D = 2 + \ln[AFpT]/\ln[b]$, but the presence of overlap increases the apparent area fraction per tier, which is reflected by the second term in the numerator of eq. (6). The overlap fraction per tier is $AFO = AF(N)*AF(N-1) \approx (AFpT)^2$.

The total area fraction of the stratified percolation plots is not uniquely defined for a given scale b and $AFpT$. Instead, it depends on the resolution and the upper cut-off of the pattern: this is a fundamental property of fractals. For n tiers, the total area fraction is given approximately by

$$AF_n \approx AFpT[AFpT + (1 - AFpT)(AFpT)^2]^{n-1}. \tag{7}$$

The results from eqs. (6) and (7) are plotted in Figures 10 and 11. Monte Carlo computer simulations were run which measured the actual area fractions and correlation functions for varying $AFpT$ and b. The estimates of eqs. (6) and (7) are essentially correct up to around four tiers. Deviations of eq. (7) from the measured area fraction occur for more than four tiers due to errors in counting overlap of structures on different tiers. Likewise the fractal dimension given in eq. (6) is found to underestimate the measured values (see eq. (9)).

Fractal stratified percolation plots are shown in Figure 12 with increasing fractal dimensions. The fractal dimensions of the plots were verified by calculating the auto-correlation functions using two-dimensional fast Fourier transforms (FFT). Aliasing in the transforms was eliminated by zero-padding, which removes the effects of the artificial periodicity imposed by the FFT algorithm. It is interesting to compare the real data of Figure 4 to the simulation in Figure 12b, both of which have similar fractal dimensions: the qualitative match of the flow path patterns is

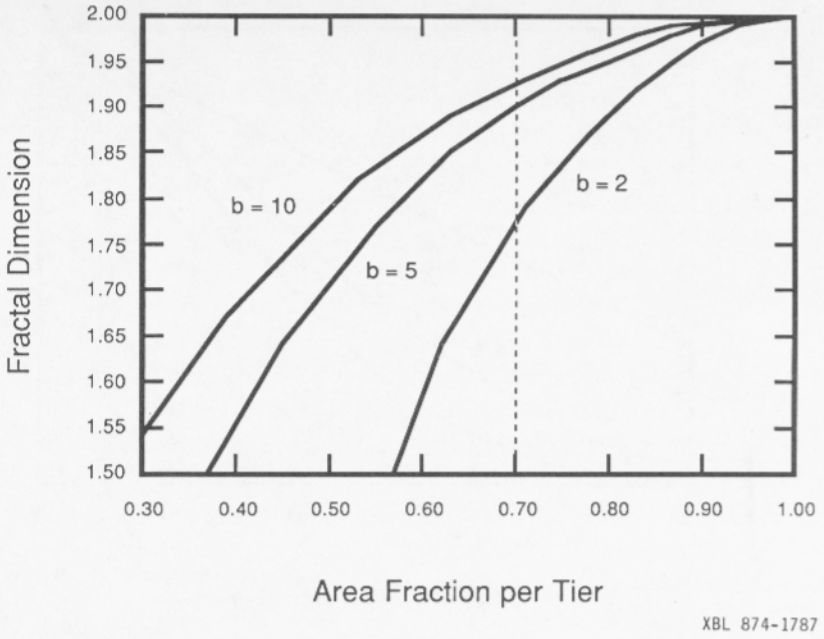

Figure 10
Approximate fractal dimensions of stratified continuum percolation models as functions of area fraction per tier (AFpT) for three values of scale parameter: $b = 2$, $b = 5$, and $b = 10$. The percolation threshold occurs near $AFpT = 0.7$, independent of the resolution (number of tiers).

quite good. Overall, the results of the stratified percolation model match well with the data of the compliant fracture E30, but do not match as well with the data of the stiff fracture E32. The area fractions are substantially different, and the large, bulky areas of contact observed in E30 do not appear in E32. Large areas of contact are still present in E32, as they must be in order to produce the fractal dimension of the pattern; however they are drawn out into thin strings and filaments with coastlines of high fractal dimension. The stratified percolation model that we have presented tends to produce bulky structures rather than filaments. This feature is directly related to the lacunarity (MANDELBROT, 1983) of the patterns. Lacunarity is a qualitative measure of the connectedness of the tremas. Large lacunarity corresponds to large and bulky tremas as in sample E30, while small lacunarity corresponds to small and fragmented tremas as in sample E32. Some additional degree of freedom should therefore be introduced into our model that would influence the lacunarity of the tremas. We do not attempt to expand the model in the present work, but feel that the gross features of the flow paths through the fracture are reasonably well explained.

The percolation properties of the stratified continuum model require some discussion. The model is based on the standard continuum model, for which the

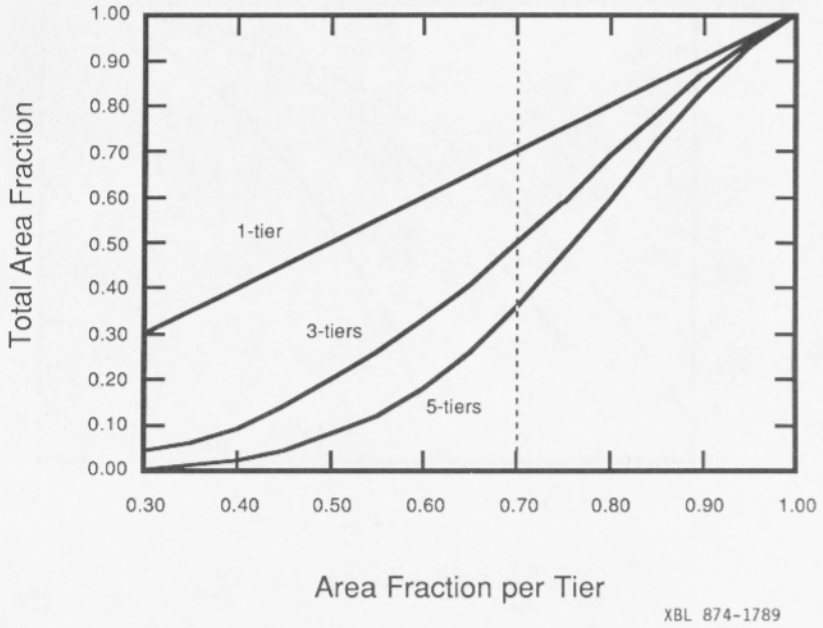

Figure 11
Approximate total area fraction as a function of $AFpT$ for a 1-tiered, 3-tiered, and 5-tiered stratified continuum percolation plot. The total area fraction is clearly a function of the number of tiers (resolution).

area fraction is the variable parameter which defines the percolation threshold and the percolation exponents. However, the total area fraction of the stratified plots is a function of the number of tiers (or the cut-off), and therefore the total area fraction is not uniquely defined. For this reason, the total area fraction of a fractal percolation model cannot be used as the critical parameter. The fractal dimension is well defined but the percolation threshold again does not occur at a uniquely defined fractal dimension: the fractal dimension can be used as an indicator of the nearness to threshold, but cannot be used quantitatively. On the other hand, the computer simulations do indicate that all the systems (for varying fractal dimension and scale factor b) have a threshold at $AFpT \approx 0.7$, which is the percolation threshold of the standard model. A well defined percolation threshold can therefore be identified for the stratified percolation simulations which use AFpT as an input parameter.

Defining the percolation threshold is of great importance for helping understand the flow properties of a random system. Near the threshold, the flow equation should be

$$Q - Q_\infty = C \cdot (d_{\max} - d)^m \cdot (AFpT - 0.7)^t \tag{8}$$

where t is the flow percolation exponent. Extensive Monte Carlo renormalization

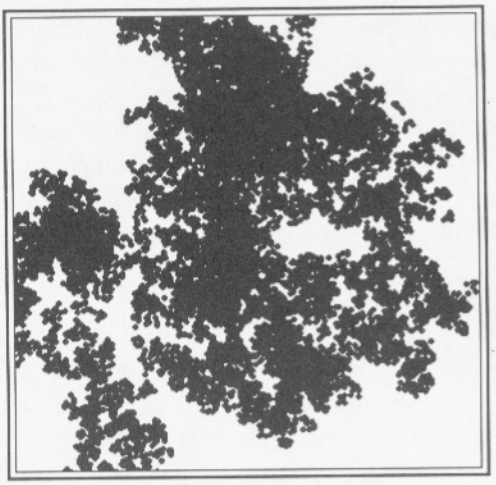

XBL 8611-4763

Fig. 12(a)

XBL 8611-4766

Fig. 12(b)

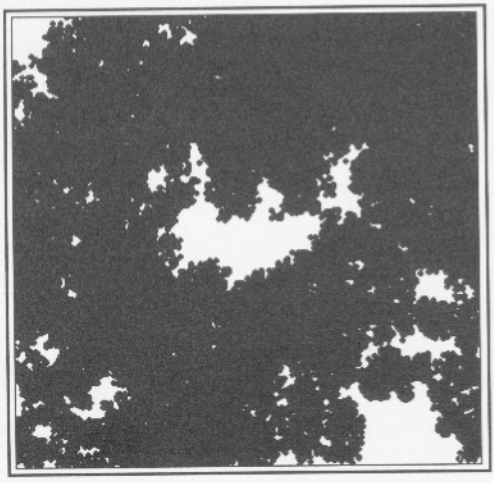

XBL 8611-4765

Fig. 12(c)

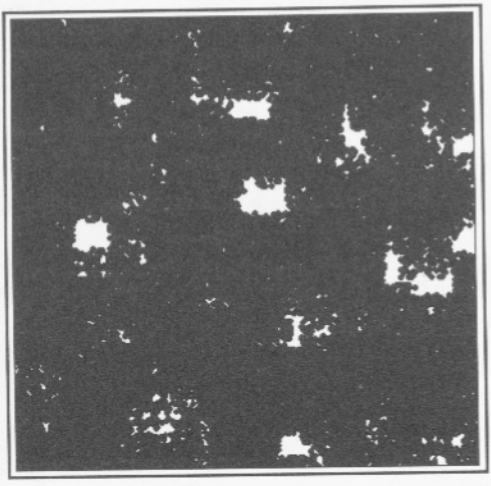

XBL 8611-4764

Fig. 12(d)

Figure 12

Stratified continuum percolation plots for a succesion of fractal dimensions: (a) 5–tiers, $b = 2.4$, 7 points per tier, area fraction per tier at the percolation limit: $AFpT = 0.70$, $D = 1.80$; (b) 5–tiers, $b = 2.4$, 9 points per tier, $AFpT = 0.79$, $D = 1.94$. This pattern should be compared with the real flow path pattern in Figure 4; (c) 5–tiers, $b = 2.4$, 10 points per tier, $AFpT = 0.89$, $D = 1.97$; (d) 2–tiers, $b = 9$, 250 points per tier, $AFpT = 0.96$, $D = 1.99$.

group analysis (REYNOLDS *et al.*, 1980) would be required to accurately determine the value of the exponent, but arguments of universality between stratified percolation and standard percolation behavior may provide an estimate for the exponent. From Figure 11 it can be seen that the total area fractions of the stratified plots depend linearly on the $AFpT$ around the threshold. Therefore the conductivity exponent of the standard model may carry over unmodified into the stratified model. As stated earlier, estimates for t in the standard continuum model range from 1.7 to 2.7 (HALPERIN *et al.*, 1985).

The conductivity of the experimentally measured flow-paths can now be described semi-quantitatively by finding the values of $AFpT$ for the various fractures and loadings. We can calculate the area fraction per tier by defining a standard resolution, or cut-off, for both the simulation and the real pattern. For the given resolution, both the fractal dimension and the total area fraction can be measured and matched to the results of stratified continuum percolation in order to determine the AFpT of the measured pattern. Comparing the calculated $AFpT$ of the real pattern to $AFpT_c \approx 0.7$ then gives a quantitative measure of the separation of the real system from the critical percolation threshold. Defining a set resolution for the patterns is paramount to setting the number of tiers used in the stratified percolation construction. Due to this imposed cut-off, the pattern no longer truly scales and measured fractal dimension is larger than the values predicted by eq. (6). To correct for the finite number of tiers, eq. (6) must be modified before the AFpT can be derived from the fractal dimension and total area fraction of the pattern. For n tiers, the measured fractal dimension of the pattern is

$$D \approx \frac{(n-1)\ln[AFpT + (1-AFpT)(AFpT)^2]}{(n)\ln[b]} + 2. \tag{9}$$

In the limit of many tiers, this expression reduces to eq. (6) which is valid for true scaling. By plotting the fractal dimension in eq. (9) against the total area fraction in eq. (7) for a given AFpT, we obtain a plot of isobars of constant AFpT. This is shown in Figure 13 with the data of samples E30 and E32 for various loads. The isobars are only plotted for $n = 1$ to $n = 5$ tiers because that is the range of validity of eqs. (7) and (9) (because of the neglect of higher orders of overlap). For $n = 1$, there is only one tier, and the fractal dimension $D = 2.00$ independent of the $AFpT$. This is the expected result of standard continuum percolation. Under the highest stress (85 MPa) the fracture in E30 has $AFpT \approx 0.8 \pm 0.1$ while the stiffer fracture in E32 has $AFpT \approx 0.7 \pm 0.1$. This places the fracture in E32 right at the percolation threshold, and the fracture in E30 within 15% of the threshold. Of course, the errors in the values of both D and AF for these fractures are reflected in the errors on $AFpT$.

For the fracture in E30 at the highest stress, the normalized conductivity from eq. (8) should be reduced roughly by a factor

$$\frac{(0.8-0.7)^{2.2}}{(1.0-0.7)^{2.2}} \approx 0.1 \tag{10}$$

from the maximum conductivity at unit area fraction. Here the exponent, 2.2, is taken as a probable value for the conductivity exponent, t. This reduction in conductivity is the result of only considering the changing flow path geometry. At the same time, the aperture is decreasing, further reducing the flow. We can now roughly estimate the exponent m in eq. (8) by comparing eqs. (8) and (10) with eq. (2) for which the exponents $n \approx 8$. For the fracture in E30, these are related by

$$0.1(b_{85}/b_0)^m = (b_{85}/b_0)^8 \tag{11}$$

where the mechanical apertures at 85 MPa and zero load are $b_{85} = 3$ microns and $b_0 = 12.5$ microns, respectively, and the factor 0.1 is the reduction in flow from increasing tortuosity from eq. (10). Solving for the exponent in eq. (11) yields $m = 6.4$. Therefore, we find that the empirical dependence of flow on large exponents of the mechanical aperture can be partially explained by explicitly

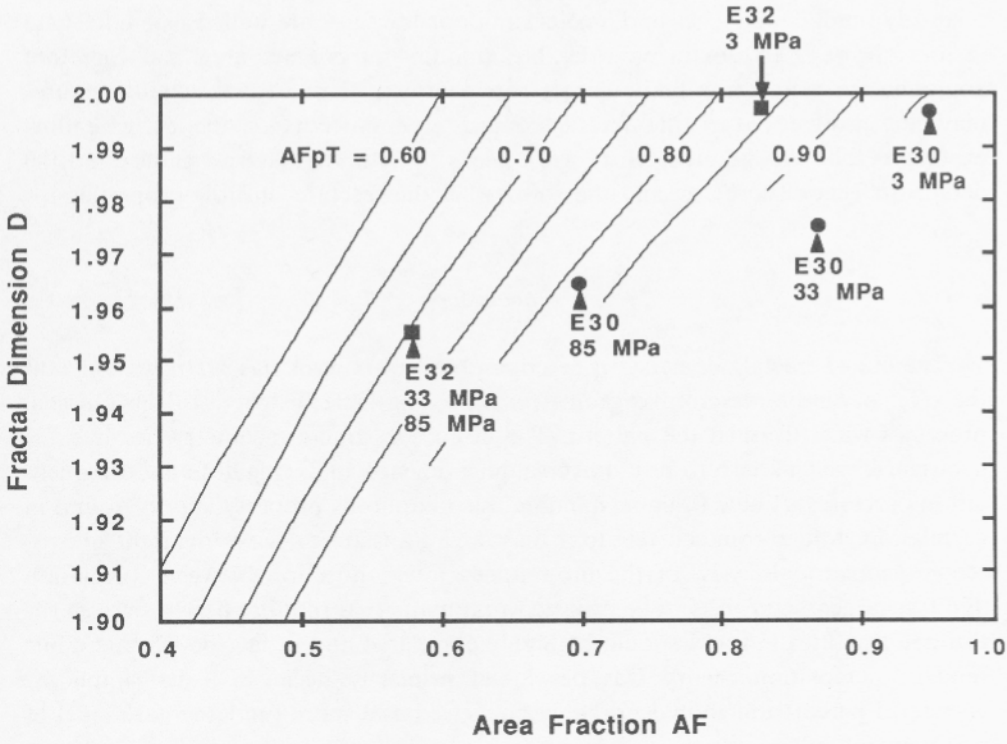

Figure 13

Fractal dimension D from eq. (9) correlated against the total area fraction AF from eq. (7). The lines are contours of constant $AFpT$ and are only plotted for one to five tiers. The fractal dimension for one tier is always $D = 2.00$. The data from the metal injection are also plotted.

considering the effects of increasing tortuosity on flow through fractures, derived from the principles of percolation theory. However, the dependence of flow on mechanical aperture alone continues to have exponents larger than cubic, which indicates that mechanical and hydraulic aperture are related in a nontrivial way.

An explanation of this remaining nontrivial relationship between mechanical and hydraulic aperture requires a detailed investigation of the specific details of the aperture distributions in the fracture and of the effect of mechanical deformation on that distribution (PYRAK-NOLTE *et al.*, 1988). In the presentation of the stratified continuum model, the *AFpT* is not assumed to be a physical quantity in a real system. However, the concept of tiers may in fact be related to the aperture distribution. Also, the continuous dependence of flow on aperture has until now been discarded in favor of a binary process in which flow is either present or not. Even at low stress a percolating critical path must exist which is highly sensitive to changes in aperture. In this sense, the effects of percolation are present at all stresses, not only at the highest stress.

Finally, we must state that we do not claim that our fluid flow and contact area data are universal properties for all natural fractures. Our core samples are relatively small (~ 2 inches in diameter) and our fractures are well registered. These factors allow us to obtain considerable amounts of contact area and therefore approach the percolation limit. Larger core samples, or poorly registered fractures may not produce either the fractal contact area patterns or the extreme flow exponents that we obtained. More work needs to be undertaken to understand the detailed effects of core size and the stiffness of the fracture on flow properties.

5. Conclusions

The use of fractal geometry to describe physical patterns has often remained at the level of simple descriptive geometry, providing little insight into the physical processes which formed the pattern. The essence of fractal geometry lies in scale invariance, which seems to be a universal phenomenon in aggregation and fragmentation processes. A clue to understanding this ubiquitous property may be found in correlation. Microscopic correlations may well translate to scale invariant macroscopic geometry. In view of the pronounced interconnection between correlation and fractal geometry, it is to be expected that many real random flow processes (as through fractures in rock) should be highly correlated and in fact be fractal. While random percolation theory was developed primarily because of its simplicity, correlated percolation should probably be viewed as a more fundamental model of real percolation processes.

Fluid flow through a fracture in rock is clearly a three-dimensional process of high geometrical complexity. Significant simplification can be achieved by decoupling the two-dimensional effects from the effects of the third, perpendicular

direction. We have described in this paper how the two-dimensional projection of the void-space geometries can be obtained by making metal casts of the fracture under varying stresses. This two-dimensional projection defines a nominal flow path which can be analyzed using two-dimensional percolation theory. While standard continuum percolation theory can define the critical area fraction for percolation, the flow path areas of the natural fractures are found to be fractal, with no well defined area fraction. A stratified, or correlated, continuum percolation model was found to give semi-quantitative agreement with the observed flow path geometries. The critical threshold in this new model was found to be related to the area fraction covered by the flow path for a given level in the iterative procedure for modelling the flow path geometry. This area fraction per tier ($AFpT$) was determined for the measured flow paths by fitting the total area fraction (at a set resolution) as well as the fractal dimension of the pattern. For this reason, the fractal dimension becomes more than a mere descriptive value: it can be used directly to evaluate the physical behavior of the flow through the natural fracture.

Acknowledgment

We gratefully acknowledge critical comments from P. Reynolds. This work was supported by the Office of Civilian Radioactive Waste Management through the Office of Geologic Repositories through U.S. DOE contract AC03-76SF00098.

References

Aharony, A. (1984), *Percolation, Fractals, and Anomalous Diffusion*, J. Stat. Phys. *34*, 931–939.

Balberg, I., Binenbaum, N., and Anderson, C. H. (1983), *Critical Behavior of the Two-dimensional Sticks System*, Phys. Rev. Lett. *51*, 1605–1608.

Bandis, S., Lumsden, A. C., and Barton, N. R. (1983), *Fundamentals of Rock Joint Deformation*, Int. J. Rock Mech. Min. Sci. and Geomech. Abstr. *20*, 249–268.

Böttger, H., and Bryskin, V. V., *Hopping Conduction in Solids* (VCH, Altenburg 1985).

Brown, S. R., and Scholz, C. H. (1985), *Closure of Random Elastic Surfaces in Contact*, J. Geophys. Res. *90*(B7), 5531–5545.

Brown, S. R., Kranz, R. L., and Bonner, B. P. (1986), *Correlation between the Surfaces of Natural Rock Joints*, Geophys. Res. Lett. *13*, 1430.

Brown, S. R. (1987), *Fluid Flow through Rock Joints: The Effect of Surface Roughness*, J. Geophys. Res. *92*(B2), 1337–1347.

Domb, C., and Green, M. S. ed., *Phase Transitions and Critical Phenomena* (Academic, London 1976).

Duncan, N., and Hancock, K. E. (1966), *The Concept of Contact Stress in Assessment of the Behavior of Rock Masses as Structural Foundations*, Proc. First Cong. Int. Soc. Rock Mech., Lisbon, 2, 487–492.

Elam, W. T., Kerstein, A. R., and Rehr, J. J. (1984), *Critical Properties of the Void Percolation Problems for Spheres*, Phys Rev. Lett. *17*, 1516–1519.

Engelder, T., and Scholz, C. H. (1981), *Fluid Flow Along Very Smooth Faults at Effective Pressures up to 200 Megapascals*, Am. Geophys. Union Monogr. *24*, 147–152.

Essam, J. W. (1980), *Percolation Theory*, Rep. Prog. Phys. *43*, 833–912.